Vibration analysis of an elastic-sphere oscillator contacting semi-infinite viscoelastic solids in resonant ultrasound microscopy

Cite as: Journal of Applied Physics **95**, 8366 (2004); https://doi.org/10.1063/1.1737472
Submitted: 01 December 2003 . Accepted: 15 March 2004 . Published Online: 04 June 2004

Jiayong Tian, Hirotsugu Ogi, and Masahiko Hirao

Vibration analysis of an elastic-sphere oscillator contacting semi-infinite viscoelastic solids in resonant ultrasound microscopy

Jiayong Tian,[a] Hirotsugu Ogi, and Masahiko Hirao
Graduate School of Engineering Science, Osaka University, Machikaneyama 1-3, Toyonaka, Osaka 560-8531, Japan

(Received 1 December 2003; accepted 15 March 2004)

Resonant-ultrasound microscopy evaluates local Young's modulus of materials by the resonant-frequency shift of a vibrating oscillator. This study presents a dynamic-contact model to analyze free vibrations of an isotropic elastic-sphere oscillator contacting two semi-infinite viscoelastic solids, which sandwich the sphere. Assuming frictionless contacts and smaller vibrational amplitude, dynamic-contact pressure distributions are obtained with the linearized maximum contact pressure and contact radius. Combining the sphere oscillation and the solid motions through contact-displacement boundary conditions, resonant frequencies of the elastic sphere are obtained. Unlike the quasistatic model, this dynamic model agrees well with the measurements. © *2004 American Institute of Physics.* [DOI: 10.1063/1.1737472]

I. INTRODUCTION

Evaluation of elastic properties in a micro- and nanoscale region of a solid is of great importance for optimization of applications including surface-wave acoustic devices and microelectromechanical systems (MEMS). It can be achieved by using the resonant-frequency shift of a vibrating oscillator contacting the solid. Typical measurement uses an atomic-force-microscope cantilever.[1] One end of the cantilever is gripped by a holder and the other end contacts the specimen surface through a small tip. A piezoelectric transducer attached to the cantilever causes a flexural vibration, while maintaining contact with the specimen. Because this approach involves many components contributing to the resonance, and the resonant frequency is highly affected by the ambiguous gripping condition, quantitative evaluation of a material's elasticity has not been straightforward. We have recently developed an alternate resonant-ultrasound-microscopy (RUM) method using an isolated piezoelectric oscillator[2–4] which aims to overcome the long-running problems associated with contact acoustic coupling. Our method does not require any acoustical contacts except for the point contact with the specimen, which allows us to quantitatively evaluate the local Young's modulus.

In such a resonant-ultrasound-microscopy measurement, the influence of material's elastic properties on the oscillator's vibration remains the central issue. Previous studies[5–9] assumed a flat contact interface between the oscillator and the specimen, replaced it with a linear spring obtained by Hertzian contact theory, and calculated the dependence of the resonant-frequency shift on the elastic constants of the material. (We call this model the quasistatic Hertzian-contact model.) Thus, this assumption neglects the influence of nonuniform vibrational deformation at the contacting interface, the mass density of the specimen, and vibrational frequency of the system. This is unphysical. Indeed, our previous study[2–4] showed that the quasistatic Hertzian-contact model failed to explain the frequency shift of an oscillator caused by contacts: the resonant-frequency shift predicted by the quasistatic model is much smaller than the observation. The same occurred in ultrasonic indentation measurements.[5] To date, no study has analyzed an elastic-oscillator vibration with contacts with viscoelastic materials considering a *dynamic* Hertzian contact.

There are three principal purposes in this study: (i) present an dynamic Hertzian-contact model to predict the free-vibration resonant frequencies of an isotropic elastic-sphere oscillator contacting semi-infinite viscoelastic solids; (ii) investigate the effect of the contacting material's moduli, mass density, and viscosity on the resonant frequencies; and (iii) confirm the developed model with measurements using an electromagnetic–acoustic–transduction method,[10] where the electromagnetic–acoustic coupling generates and detects the vibration of the sphere without any contact.

Our analysis proceeds in four steps. First, assuming small vibrational amplitude, the approximate dynamic-contact-pressure distributions are presented (Sec. II A). Second, vibration of an elastic sphere subjected to dynamic contact pressure is analyzed in spherical coordinates (Sec. II B). Third, the motion of semi-infinite viscoelastic solids subjected to dynamic contact pressure at the contacting surface is analyzed using Hankel transforms in cylindrical coordinates (Sec. II C). Fourth, the resonant frequencies of the overall system are derived by combining two solutions at the contact area through the dynamic-contact boundary conditions for displacements (Secs. II D and E). The present analysis showed good agreement with the measurements of the resonant-frequency shifts, indicating the necessity of considering the dynamic response near the contacting area in the resonant-ultrasound microscopy.

[a]Electronic mail: j_tian@me.es.osaka-u.ac.jp

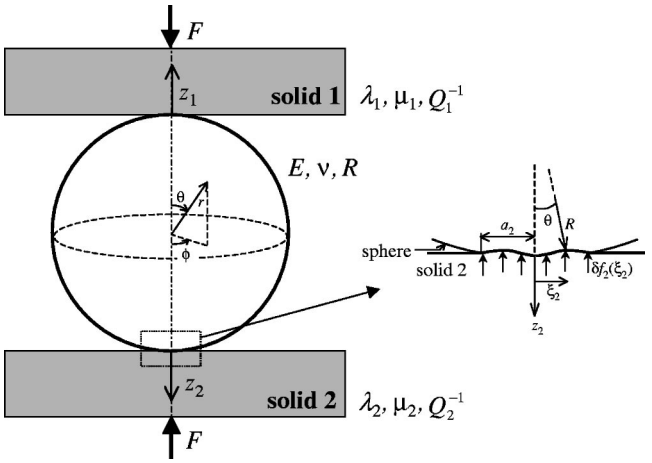

FIG. 1. A dynamic model of an elastic sphere contacting two semi-infinite viscoelastic solids.

II. RESONANT FREQUENCY OF AN ELASTIC SPHERE CONTACTING SEMI-INFINITE VISCOELASTIC SOLIDS

Various types of oscillators such as spheres, cantilevers, and rectangular parallelepipeds can be used in resonant-ultrasound microscopy. Because the principal aim of this study is to investigate mathematically the influence of the dynamic contacting response on the resonant frequency of an oscillator, we consider the simplest oscillator, a sphere.

Consider an isotropic elastic sphere with radius R, Young's modulus E, and Poisson's ratio ν in frictionless contact with two semi-infinite viscoelastic solids, as shown in Fig. 1. (This model includes the case of one-point contact with $\lambda_1 = \mu_1 = 0$.) The stress–strain relationships in the viscoelastic solids take the form[11]

$$\sigma_{ij} = \lambda_n (1 + iQ_n^{-1}) e \delta_{ij} + \mu_n (1 + iQ_n^{-1}) \epsilon_{ij}. \tag{1}$$

Here, the subscript $n(=1 \text{ or } 2)$ indicates the solid (solid 1 or solid 2). λ_n and μ_n are Lamé constants of the solids. σ_{ij} and ϵ_{ij} are stress and strain of the solids, respectively; $e = \epsilon_{11} + \epsilon_{22} + \epsilon_{33}$; δ_{ij} is Kronecker's delta symbol. Q_n^{-1} denotes internal friction of the solids. (There are usually two independent internal friction associated with λ and μ, respectively, in an isotropic material, but we assume the same value for them to simplify the problem. This assumption affects the resulting resonant frequencies, but little, as shown later.) Also, we assume that the vibrational amplitude of the elastic sphere is much smaller than the indentation caused by the static biasing force.

A. Dynamic contact stress distribution at the sphere–solid interfaces

A static normal force F pressing the sphere and two solids together results in circular contact areas, whose radii are expressed as[12]

$$a_n = \sqrt[3]{\frac{3FR}{4E_n^*}}. \tag{2}$$

Here, E_n^* denotes the effective Young's modulus of the contacting sphere and solids, satisfying $1/E_n^* = [(1-\nu^2)/E] + [(1-\nu_n^2)/E_n]$. E_n and ν_n are Young's modulus and Poisson's ratio of the solid 1 or 2, respectively.

The normal contact pressure distribution $p_n(\xi_n)$, expressed in the local cylindrical coordinate system (ξ_n, z_n) shown in Fig. 1, is given by[12]

$$p_n(\xi_n) = p_n \sqrt{1 - \xi_n^2/a_n^2}, \tag{3}$$

where $p_n = 3F/2\pi a_n^2$ denotes the maximum static pressure.

The harmonic vibration of the elastic sphere will change the contact-pressure distribution and the contact radius. We assume that the general form of Eq. (3) still holds for such a time-dependent problem

$$p_n(\xi_n, t) = p_n(t) \sqrt{1 - \xi_n^2/a_n(t)^2}, \tag{4}$$

where $p_n(t)$ and $a_n(t)$ denote the maximum dynamic pressure and dynamic contact radius, respectively; they depend on time t. They will be implicitly determined later by the boundary conditions for deformation (see Sec. II D). We rewrite Eq. (4) as

$$p_n(\xi_n, t) = (p_n + \delta p_n(t)) \sqrt{1 - \xi_n^2/(a_n + \delta a_n(t))^2}, \tag{5}$$

where $\delta p_n(t)$ and $\delta a_n(t)$ are unknown perturbations to the static values p_n and a_n, respectively. $\delta p_n(t)$ and $\delta a_n(t)$ can be approximated to be harmonic oscillations with the angular frequency ω

$$\left.\begin{aligned} \delta p_n(t) &\approx \delta p_n e^{i\omega t} \\ \delta a_n(t) &\approx \delta a_n e^{i\omega t} \end{aligned}\right\}, \tag{6}$$

where δp_n and δa_n are unknown constants and we assume $|\delta p_n| \ll p_n$ and $|\delta a_n| \ll a_n$. In Eq. (6), we neglect the influence of internal friction of the solids for two reasons: (i) The contact area and vibrational amplitude of the sphere are much smaller than the wavelength, and the effect of internal friction on the interface spring constants will be small. (ii) Incorporation of internal friction in Eq. (6) results in a labyrinth of relationships among the related properties and makes it impossible to solve the system mathematically. We consider the effect of internal friciton in vibrational analysis in the solids in Sec. B and will show that it little affects the resonance frequencies of the system.

Substitution of Eq. (6) into Eq. (5) leads to

$$p_n(\xi_n, t) \approx p_n \sqrt{1 - \xi_n^2/a_n^2} + \delta f_n(\xi_n) e^{i\omega t}, \tag{7}$$

by retaining the first-order perturbations. The second term of Eq. (7) denotes the harmonic contact-pressure distribution due to the sphere vibration given by

$$\delta f_n(\xi_n) = p_n \frac{\xi_n^2 \delta a_n}{a_n^3 \sqrt{1 - \xi_n^2/a_n^2}} + \delta p_n \sqrt{1 - \xi_n^2/a_n^2}. \tag{8}$$

Thus, the nonlinear-contact problem with the dynamic contact radius is reduced to a linear problem. Equation (7) indicates that the system can be expressed by a linear superposition of a static problem related to the Hertzian contact and a dynamic problem with harmonic contact pressure $\delta f_n(\xi_n) e^{i\omega t}$ at the interfaces. We only consider the dynamic response in the following analysis.

B. Elastic sphere subjected to harmonic contact pressure

We next consider the dynamic response of the elastic sphere subjected to harmonic contact pressure, $\delta f_n(\xi_n)e^{i\omega t}$. The factor $e^{i\omega t}$ will be omitted for brevity. Free vibration of an isotropic elastic sphere without any contacts falls into two vibration groups, torsional modes and spheroidal modes.[13] Torsional modes do not have any radial displacements, but spheroidal modes do. We consider only the spheroidal modes because, in resonant-ultrasound microscopy, they show much larger sensitivity to the elastic constants of solids than torsional modes, where a biasing force is vertically applied.

Equations of motion for the harmonic spheroidal vibration in the spherical coordinates system (r,θ,ϕ) shown in Fig. 1 are expressed as[13]

$$\left.\begin{aligned}&\nabla^2\varphi+k_L^2\varphi=0, \quad k_L=\frac{\omega}{v_L}\\ &\nabla^2\chi+k_S^2\chi=0, \quad k_S=\frac{\omega}{v_S}\end{aligned}\right\}, \tag{9}$$

where φ and χ denote the displacement potentials. $v_L=\sqrt{(\lambda+2\mu)/\rho}$ and $v_S=\sqrt{\mu/\rho}$ are the longitudial and shear-wave velocities of the elastic sphere, respectively. λ, μ, and ρ are Lamé constants and mass density of the sphere.

The general solutions of Eq. (9) are expressed as[13]

$$\left.\begin{aligned}&\varphi=c_{ml}j_m(k_Lr)P_m^l(\cos\theta)e^{il\phi}\\ &\chi=d_{ml}j_m(k_Sr)P_m^l(\cos\theta)e^{il\phi}\end{aligned}\right\}, \tag{10}$$

where c_{ml} and d_{ml} are unknown constants. j_m and P_m^l denote the spherical Bessel function and the associated Legendre functions with the colatitudinal mode number m and the azimuthal mode number l, respectively. We only consider the case that $l=0$ for two reasons: (i) As shown later, the electromagnetic–acoustic–resonance microscopy used in the present study causes principally the vibration modes of $l=0$, and (ii) The contact pressure is axisymmetric about the z axis. Thus, the displacement potentials are independent of ϕ.

The displacements and stresses are obtained from the equations for φ and χ that are presented in Appendix A

$$\left.\begin{aligned}u_r(r,\theta,\phi)&=(c_{m0}C_{m1}(r)+d_{m0}D_{m1}(r))P_m^0(\cos\theta)\\ u_\theta(r,\theta,\phi)&=(c_{m0}C_{m2}(r)+d_{m0}D_{m2}(r))\frac{dP_m^0(\cos\theta)}{d\theta}\\ u_\phi(r,\theta,\phi)&=(c_{m0}C_{m3}(r)+d_{m0}D_{m3}(r))\frac{P_m^0(\cos\theta)}{\sin\theta}\end{aligned}\right\}, \tag{11}$$

$$\left.\begin{aligned}\sigma_{rr}(r,\theta,\phi)&=(c_{m0}C_{m4}(r)+d_{m0}D_{m4}(r))P_m^0(\cos\theta)\\ \sigma_{r\theta}(r,\theta,\phi)&=(c_{m0}C_{m5}(r)+d_{m0}D_{m5}(r))\frac{dP_m^0(\cos\theta)}{d\theta}\\ \sigma_{r\phi}(r,\theta,\phi)&=(c_{m0}C_{m6}(r)+d_{m0}D_{m6}(r))\frac{P_m^0(\cos\theta)}{r^2\sin\theta}\end{aligned}\right\}, \tag{12}$$

where $C_{m1}(r)-C_{m6}(r)$ and $D_{m1}(r)-D_{m6}(r)$ are shown in Appendix B. [Note that displacements and stresses in Eqs. (11) and (12) are time-dependent quantities.] Boundary conditions at the surface $r=R$ are represented by

$$\sigma_{rr}(R,\theta,\phi)=\begin{cases}-\delta f_1(\xi_1) & 0\leqslant\theta\leqslant\dfrac{a_1}{R}\\ -\delta f_2(\xi_2) & \pi-\dfrac{a_2}{R}\leqslant\theta\leqslant\pi\\ 0 & \dfrac{a_1}{R}\leqslant\theta\leqslant\pi-\dfrac{a_2}{R}\end{cases}$$

$$\sigma_{r\theta}(R,\theta,\phi)=0 \tag{13}$$

$$\sigma_{r\phi}(R,\theta,\phi)=0.$$

We expand the stress at the surface of the sphere using the spherical harmonics functions[14]

$$\sigma_{rr}(R,\theta,\phi)=-\sum_{m=0}^{\infty}\sum_{l=-m}^{m}B_{ml}P_m^l(\cos\theta)e^{il\phi}, \tag{14a}$$

where

$$B_{ml}=\frac{2l+1}{4\pi}\int_0^{\pi}\int_0^{2\pi}\sigma_{rr}(R,\theta,\phi)P_m^l(\cos\theta)\sin\theta e^{-il\phi}d\phi\,d\theta. \tag{14b}$$

Combination of Eqs. (8), (13), and (14b) leads to

$$B_{ml}=\begin{cases}\delta p_1N_1+\delta a_1N_2+\delta p_2N_3+\delta a_2N_4, & l=0\\ 0, & l\neq0,\end{cases} \tag{14c}$$

$$N_1=\frac{(2m+1)a_1^2}{6R^2}, \tag{14d}$$

$$N_2=\frac{(2m+1)p_1}{2a_1^3}\int_0^{a_1/R}\frac{R^2\theta^2}{\sqrt{1-R^2\theta^2/a_1^2}}P_m^0(\cos\theta)\sin\theta d\theta, \tag{14e}$$

$$N_3=\frac{(-1)^m(2m+1)a_2^2}{6R^2}, \tag{14f}$$

$$N_4=\frac{(2m+1)p_2}{2a_2^3}\int_{\pi-(a_2/R)}^{\pi}\frac{R^2(\pi-\theta)^2}{\sqrt{1-R^2(\pi-\theta)^2/a_2^2}}\times P_m^0(\cos\theta)\sin\theta\,d\theta. \tag{14g}$$

C. Dynamic response of semi-infinite viscoelastic solids subjected to harmonic contact pressure

Here, we study the dynamic response in the visoelastic solids subjected to the harmonic contact pressure, $\delta f_n(\xi_n)$. Because of the circular contact area and axisymmetric contact pressure, the dynamic response is solved in cylindrical coordinates (ξ_n,z_n) shown in Fig. 1. Nonzero displacement components $u_{\xi n}(\xi_n,z_n)$ and $u_{zn}(\xi_n,z_n)$ are expressed by[11,15–18]

$$\left.\begin{aligned}u_{\xi n}&=\frac{\partial\phi_n}{\partial\xi_n}+\frac{\partial^2\psi_n}{\partial\xi_n\partial z_n}\\ u_{zn}&=\frac{\partial\phi_n}{\partial z_n}-\frac{\partial^2\psi_n}{\partial\xi_n^2}-\frac{\partial\psi_n}{\xi_n\partial\xi_n}\end{aligned}\right\}, \tag{15}$$

where ϕ_n and ψ_n are the potentials satisfying the following equations:[11]

$$\left.\begin{aligned}(1+iQ_n^{-1})\nabla^2\phi_n+k_{Ln}^2\phi_n=0,\quad k_{Ln}=\frac{\omega}{v_{Ln}}\\(1+iQ_n^{-1})\nabla^2\psi_n+k_{Sn}^2\psi_n=0,\quad k_{Sn}=\frac{\omega}{v_{Sn}}\end{aligned}\right\}. \tag{16}$$

Here, $v_{Ln}=\sqrt{(\lambda_n+2\mu_n)/\rho_n}$ and $v_{Sn}=\sqrt{\mu_n/\rho_n}$. Resulting stress components are[11]

$$\left.\begin{aligned}\sigma_{zzn}&=-\lambda_n k_{Ln}^2\phi_n+2\mu_n(1+iQ_n^{-1})\\&\quad\times\left(\frac{\partial^2\phi_n}{\partial z_n^2}+\frac{\partial^3\psi_n}{\partial z_n^3}+\frac{k_{Sn}^2}{(1+iQ_n^{-1})}\frac{\partial\psi_n}{\partial z_n}\right)\\\sigma_{z\xi n}&=\mu_n(1+iQ_n^{-1})\\&\quad\times\left(2\frac{\partial^2\phi_n}{\partial\xi_n\partial z_n}+2\frac{\partial^3\psi_n}{\partial\xi_n\partial z_n^2}+\frac{k_{Sn}^2}{(1+iQ_n^{-1})}\frac{\partial\psi_n}{\partial\xi_n}\right)\end{aligned}\right\}. \tag{17}$$

The boundary conditions at $z_n=0$ are given by

$$\left.\begin{aligned}\sigma_{zzn}&=\begin{cases}-\delta f_n(\xi_n) & \xi_n\leqslant a_n\\0 & \xi_n\geqslant a_n\end{cases}\\\sigma_{z\xi n}&=0\end{aligned}\right\}. \tag{18}$$

We apply Hankel transforms to this problem, which are defined as

$$\left.\begin{aligned}\hat{F}^{Hs}(q)&=\int_0^\infty F(\xi_n)\xi_n J_s(q\xi_n)d\xi_n\\F(\xi_n)&=\int_0^\infty \hat{F}^{Hs}(q)qJ_s(q\xi_n)dq\end{aligned}\right\}, \tag{19}$$

where $J_s(x)$ denotes the sth Bessel function of the first kind.

The application of Hankel transforms to Eqs. (16)–(18) yields

$$\left.\begin{aligned}\frac{d^2\hat{\phi}_n^{H0}}{dz^2}-\alpha_n^2\hat{\phi}_n^{H0}=0,\quad \alpha_n^2=q^2-\frac{k_{Ln}^2}{(1+iQ_n^{-1})}\\\frac{d^2\hat{\psi}_n^{H0}}{dz^2}-\beta_n^2\hat{\psi}_n^{H0}=0,\quad \beta_n^2=q^2-\frac{k_{Sn}^2}{(1+iQ_n^{-1})}\end{aligned}\right\}, \tag{20}$$

$$\left.\begin{aligned}\hat{u}_{rn}^{H1}&=-q\left(\hat{\phi}_n^{H0}+\frac{\partial\hat{\psi}_n^{H0}}{\partial z_n}\right)\\\hat{u}_{zn}^{H0}&=\frac{\partial\hat{\phi}_n^{H0}}{\partial z_n}+\frac{\partial^2\hat{\psi}_n^{H0}}{\partial z_n}+k_{Sn}^2\hat{\psi}_n^{H0}\end{aligned}\right\}, \tag{21}$$

$$\left.\begin{aligned}\hat{\sigma}_{zzn}^{H0}&=-\lambda_n k_{Ln}^2\hat{\phi}_n^{H0}+2\mu_n(1+iQ_n^{-1})\\&\quad\times\left(\frac{\partial^2\hat{\phi}_n^{H0}}{\partial z_n^2}+\frac{\partial^3\hat{\psi}_n^{H0}}{\partial z_n^3}+\frac{k_{Sn}^2}{(1+iQ_n^{-1})}\frac{\partial\hat{\psi}_n^{H0}}{\partial z_n}\right)\\\hat{\sigma}_{zrn}^{H1}&=-\mu_n q(1+iQ_n^{-1})\\&\quad\times\left(2\frac{\partial\hat{\phi}_n^{H0}}{\partial z_n}+2\frac{\partial^2\hat{\psi}_n^{H0}}{\partial z_n^2}+\frac{k_{Sn}^2}{(1+iQ_n^{-1})}\hat{\psi}_n^{H0}\right)\end{aligned}\right\}, \tag{22}$$

$$\left.\begin{aligned}\hat{\sigma}_{zzn}^{H0}|_{z=0}&=\delta p_n\Delta_{1n}(q)-\delta a_n\Delta_{2n}(q)\\\hat{\sigma}_{zrn}^{H1}|_{z=0}&=0\end{aligned}\right\}, \tag{23}$$

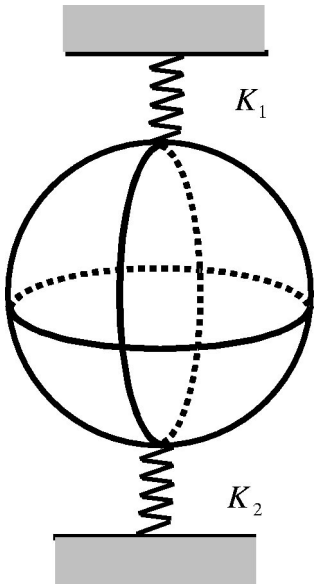

FIG. 2. Quasistatic model.

where

$$\left.\begin{aligned}\Delta_{1n}(q)&=\frac{\cos(a_nq)a_nq-\sin(a_nq)}{a_nq^3}\\\Delta_{2n}(q)&=\frac{p_n(\cos(a_nq)a_nq-\sin(a_nq)+\sin(a_nq)a_n^2q^2)}{a_n^2q^3}\end{aligned}\right\}. \tag{24}$$

Solutions of Eq. (20) that are finite at $z\to\infty$ are obtained by

$$\left.\begin{aligned}\hat{\phi}_n^{H0}&=Ae^{-\alpha_n z_n}\\\hat{\psi}_n^{H0}&=Be^{-\beta_n z_n}\end{aligned}\right\}, \tag{25}$$

where coefficients A and B are functions of q and are determined by the boundary conditions

$$\begin{aligned}\begin{bmatrix}A\\B\end{bmatrix}&=\frac{1}{\mu_n\Gamma_n(q)(1+iQ_n^{-1})}\begin{bmatrix}q^2+\beta_n^2\\2\alpha_n\end{bmatrix}\\&\quad\times(\delta p_n\Delta_{1n}(q)-\delta a_n\Delta_{2n}(q)),\end{aligned} \tag{26}$$

with

$$\Gamma_n(q)=(q^2+\beta_n^2)^2-4q^2\alpha_n\beta_n. \tag{27}$$

Substituting Eq. (25) into Eq. (21), the displacement component $\hat{u}_{zn}^{H0}(q,z_n)$ at the surface $z_n=0$ is given as

$$\begin{aligned}\hat{u}_{zn}^{H0}(q,0)&=\frac{\alpha_n k_{Sn}^2}{\mu_n\Gamma_n(q)(1+iQ_n^{-1})^2}\\&\quad\times(\delta p_n\Delta_{1n}(q)-\delta a_n\Delta_{2n}(q)).\end{aligned} \tag{28}$$

Application of the inverse Hankel transform of zero order to Eq. (28) yields

$$u_{zn}(\xi_n,0)=\delta p_n N_{1n}(\xi_n)-\delta a_n N_{2n}(\xi_n), \tag{29}$$

where

$$\left.\begin{aligned} N_{1n}(\xi_n) &= \int_0^\infty \frac{\alpha_n k_{Sn}^2}{\mu_n \Gamma_n(q)(1+iQ_n^{-1})^2}\Delta_{1n}(q) q J_0(q\xi_n) dq \\ N_{2n}(\xi_n) &= \int_0^\infty \frac{\alpha_n k_{Sn}^2}{\mu_n \Gamma_n(q)(1+iQ_n^{-1})^2}\Delta_{2n}(q) q J_0(q\xi_n) dq \end{aligned}\right\}. \tag{30}$$

Here, $N_{1n}(\xi_n)$ and $N_{2n}(\xi_n)$ are obtained numerically.

D. Contact boundary conditions for displacement

We now combine the sphere's vibration and solid's motions through the dynamic contact boundary conditions for displacements, which are given approximately according to Hertzian-contact theory[12]

$$\left.\begin{aligned} u_{z1}(0,0) - u_r(R,0,\phi) &= 0 \\ u_{z1}(a_1,0) - u_r(R, a_1/R, \phi) &= 0 \end{aligned}\right\}, \tag{31}$$

$$\left.\begin{aligned} u_{z2}(0,0) - u_r(R,\pi,\phi) &= 0 \\ u_{z2}(a_2,0) - u_r(R, \pi - a_2/R, \phi) &= 0 \end{aligned}\right\}. \tag{32}$$

From the above conditions, δp_1, δa_1, δp_2, and δa_2 are obtained as

$$\left.\begin{aligned} \delta p_1 &= T_{m1} c_{m0} + S_{m1} d_{m0} \\ \delta a_1 &= T_{m2} c_{m0} + S_{m2} d_{m0} \\ \delta p_2 &= T_{m3} c_{m0} + S_{m3} d_{m0} \\ \delta a_2 &= T_{m4} c_{m0} + S_{m4} d_{m0} \end{aligned}\right\}, \tag{33}$$

where $T_{m1} - T_{m4}$ and $S_{m1} - S_{m4}$ appear in Appendix C.

E. Resonant frequencies

Combination of Eqs. (13), (14), and (33) leads to

$$\mathbf{MX} = 0, \tag{34}$$

where

$$\mathbf{X} = [c_{m0}, d_{m0}],$$

$$\mathbf{M} = \begin{bmatrix} C_{m4}(R) + T_{m1}N_1 + T_{m2}N_2 + T_{m3}N_3 + T_{m4}N_4 & D_{m4}(R) + S_{m1}N_1 + S_{m2}N_2 + S_{m3}N_3 + S_{m4}N_4 \\ C_{m5}(R) & D_{m5}(R) \end{bmatrix}.$$

The vibration of the elastic sphere contacting two viscoelastic solids is damped and we adopt the complex frequency to solve resonant frequencies of the elastic sphere[19]

$$\tilde{\omega} = \omega(1 + i\epsilon), \tag{35}$$

where ω is the real part of the complex frequency and $\epsilon \ll 1$. Resonant frequencies of the elastic sphere are given by solving Eq. (36)

$$\det(\mathbf{M}) = 0. \tag{36}$$

For a given m, there are an infinite number of modes denoted by $S_{m,i}$ with a subscript i for the higher orders.

III. QUASISTATIC MODEL

The quasistatic model shown in Fig. 2 was often used in ultrasonic hardness tests and previous analysis in resonant-ultrasound microscopy, where the contacts between the sphere and solids were considered to be elastic springs. Here we compare this conventional model with the present dynamic model. According to Hertz theory, the spring stiffness is[12]

$$K_n = \sqrt[3]{6FRE_n^{*2}}. \tag{37}$$

Using the boundary condition at the sphere surface

$$\sigma_{rr}(R,\theta,\phi) = \begin{cases} -\dfrac{K_1 u_r(R,\theta_0,\phi)\,\delta(\cos\theta - \cos\theta_0)}{2\pi R^2} & \text{at } \theta_0 = 0 \\ -\dfrac{K_2 u_r(R,\theta_0,\phi)\,\delta(\cos\theta - \cos\theta_0)}{2\pi R^2} & \text{at } \theta_0 = \pi \end{cases}, \tag{38}$$

the resonant frequencies are obtained through

$$\det(\mathbf{N}) = 0, \tag{39}$$

where

$$\mathbf{N} = \begin{bmatrix} C_{m4}(R) + \dfrac{(K_1+K_2)C_{m1}(R)(2m+1)}{4\pi R^2} & D_{m4}(R) + \dfrac{(K_1+K_2)D_{m1}(R)(2m+1)}{4\pi R^2} \\ C_{m5}(R) & D_{m5}(R) \end{bmatrix}.$$

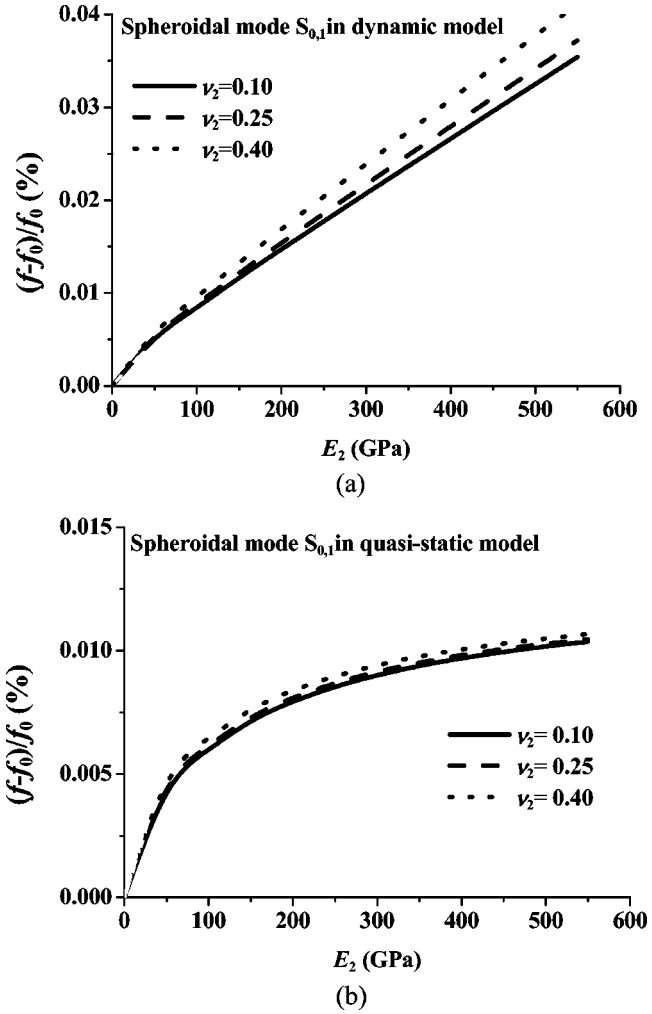

FIG. 3. Resonant-frequency shift of mode $S_{0,1}$ caused by the one-point contact as a function of Young's modulus of the contacting material with various Poisson's ratio. f_0 denotes the resonant frequency of spheroidal mode $S_{0,1}$ for the elastic sphere without any contact. (a) Dynamic model. (b) Quasistatic model. $F_0=0.18$ N, $E=196.2$ GPa, $\nu=0.29$, $R=2.4$ mm, $\rho=7942.6$ kg/m^3, $\nu_2=0.29$, $\rho_2=7800$ kg/m^3, $Q_2^{-1}=0.02$.

IV. RESULTS AND DISCUSSION: THE CASE OF ONE-POINT CONTACT

First, we consider the influence of the one-point contact with $\lambda_1=\mu_1=0$ on mode $S_{0,1}$, which is the most important mode in an actual microscopic measurement. The spheroidal modes with $m=0$ are known as radial modes because their displacements are along the radial direction. Figures 3(a) and (b) show the resonant-frequency shift caused by the contact as a function of Young's modulus and Poisson's ratio of the contacting material. The resonant frequency increases with the increase of Young's modulus and Poisson's ratio, reflecting the increase of the effective modulus E^*. Note that the dynamic model [Fig. 3(a)] always provides a frequency shift larger than that of the quasistatic model [Fig. 3(b)]. Their difference increases with the Young modulus; it reaches a factor of 4 at $E_2=550$ GPa. Furthermore, Poisson's ratio has much more influence on the resonant frequency in the dynamic model than in the quasistatic model. Thus, the dynamic model predicts higher sensitivity to the modulus of the specimen, which agrees with previous measurements[3,4] and the measurement shown later. One may attribute the larger frequency shifts in the dynamic model to the influence of the mass density and internal friction of the solid, because they do not appear in the quasistatic model. We calculated variations in the resonant frequency as a function of the mass density and internal friction in Figs. 4 and 5, respectively. They can affect the resonant frequency, but their effects are negligible. Thus, the mass density and internal friction are not principal factors for the larger frequency shifts in the dynamic model. We attribute this to the deformation distribution at the interface: the quasistatic model assumes a planar deformation. However, the actual deformation at the interface caused by vibration is more complicated, which includes a nonplanar deformation and shows larger resistance to deformation, giving rise to a larger contact stiffness. The dynamic model includes the nonplanar deformation at the interface.

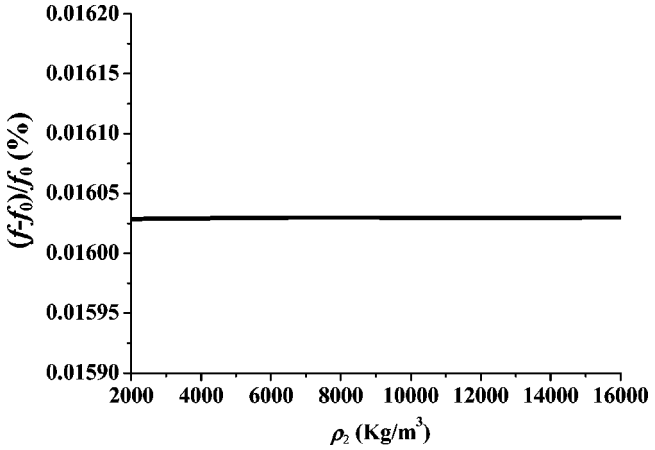

FIG. 4. Resonant-frequency shift of mode $S_{0,1}$ as a function of mass density of the contacting material for the case of one-point contact. $F_0=0.18$ N, $E=196.2$ GPa, $\nu=0.29$, $R=2.4$ mm, $\dot{\rho}=7942.6$ kg/m^3, $E_2=210$ GPa, $\nu_2=0.29$, $Q_2^{-1}=0.02$.

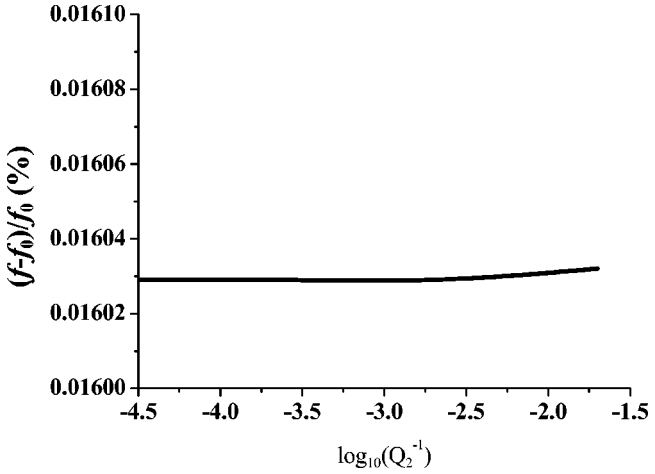

FIG. 5. Resonant-frequency shift of mode $S_{0,1}$ as a function of internal friction of the contacting material for the case of one-point contact. $F_0=0.18$ N, $E=196.2$ GPa, $\nu=0.29$, $R=2.4$ mm, $\rho=7942.6$ kg/m^3, $E_2=210$ GPa, $\nu_2=0.29$, $\rho_2=7800$ kg/m^3.

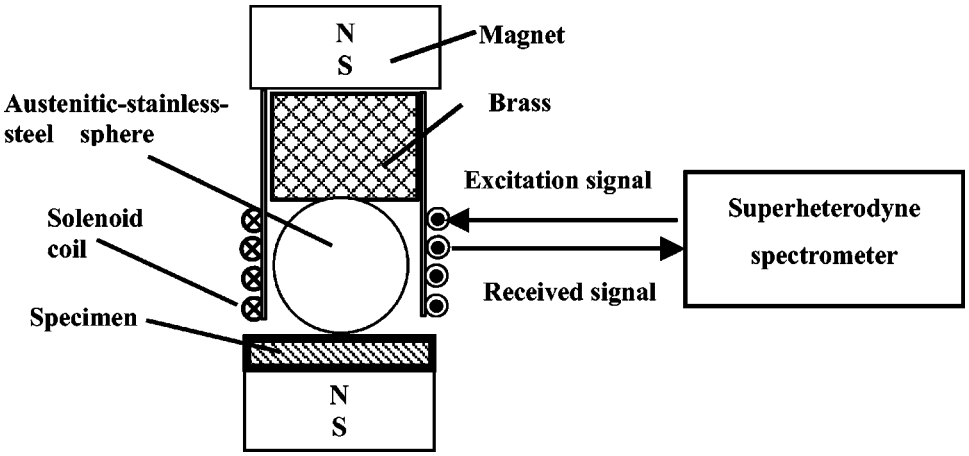

FIG. 6. The measurement setup of an electromagnetic–acoustic microscopy.

V. EXPERIMENTS

In order to verify our calculation quantitatively, we used the electromagnetic–acoustic transduction method[10] to measure the resonant frequencies of an elastic sphere. The measurement setup is shown in Fig. 6; it is essentially the same as that proposed by Johnson *et al.*[10,20] An austenitic-stainless-steel sphere with a radius of 2.4 mm and a mass density of 7942.6 kg/m^3 was inserted into a solenoid coil located between two permanent-magnet blocks. Young's modulus and Poisson's ratio of the sphere were determined to be $E=196.2$ GPa and $\nu=0.292$ by the electromagnetic–acoustic–resonance (EMAR) method.[21–23] A polycrystalline brass of 0.018 kg was located on the top surface of the sphere. The specimen was located below the sphere. Because the brass cover and the specimen were much larger than the contact areas, they can be considered as approximate semi-infinite solids. The solenoidal coil driven with high-power rf bursts causes eddy currents that are localized near the surface of the sphere. Because of the interaction of eddy currents with the static magnetic field from the permanent magnets, Lorentz forces oscillating at the same frequency as the driving bursts are generated along the radial direction to excite the spheroidal vibration of the sphere. The same coil receives the vibrational signals by the reversed-Lorentz-force mechanism. The received signals are fed to superheterodyne phase detectors to obtain the amplitude spectrum. A single frequency scan can provide many resonant peaks.

Figure 7 shows the measured free-vibration resonant spectrum of the sphere without any contact. Only three spheroidal modes maked as $S_{2,1}$, $S_{0,1}$ and $S_{2,2}$ appear in the resonant spectrum. The displacements of spheroidal modes with $m=2$ are not only along the radial direction but also the tangential direction.

Numerical calculation was done to predict the frequency shift. The parameters used in the calculation are shown in Table I. Figure 8 compares the calculation and the measurements for the spheroidal mode $S_{0,1}$. We used acrylic resin, (001) monocrystal silicon, polycrystalline boron, and polycrystalline tungsten carbide as solid 2 (specimen). The measurements appear more consistent with the dynamic model than the previous quasistatic model, which predicts much smaller frequency shift. Their difference increases with Young's modulus of the specimen.

Figure 9 shows the calculated resonant-frequency shifts for spheroidal mode $S_{2,1}$ and $S_{2,2}$ as functions of Young's modulus of solid 2. When the sphere contacts the specimens, the spectrum splits and these modes are sometimes absent from the resonant spectrum. We attribute it to the high damping of the polycrystalline brass. Hence, we failed to measure their frequency shift by the contact. The comparison between dynamic and quasistatic models for them again indicates the larger frequency shift in the dynamic model. Note that the resonant frequency of mode $S_{2,1}$ is much more sensitive to the specimen's Young's modulus than $S_{2,2}$ and $S_{0,1}$ modes.

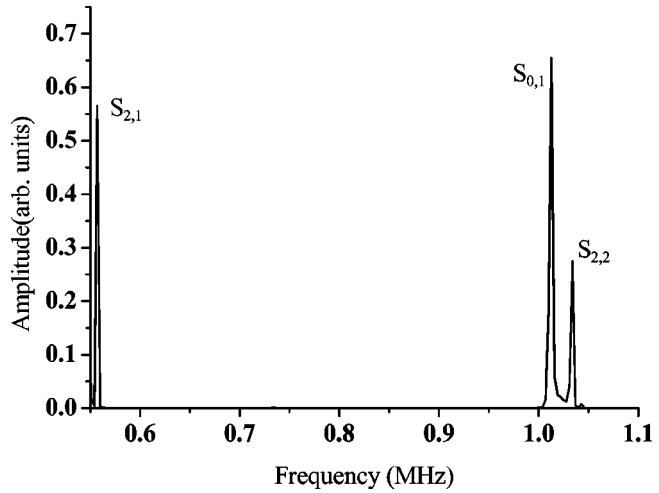

FIG. 7. Free-vibration resonant spectrum of an austenitic-stainless steel measured by an electromagnetic–acoustic transducer.

TABLE I. Material properties used in the calculation.

Materials	E (GPa)	ρ (Kg/m^3)	ν
Acrylic resin	2.9	1 900	0.41
(001) monocrystal silicon	110	2 300	0.24
Polycrystalline brass	130	8 300	0.35
Polycrystalline boron	400	2 500	0.25
Polycrystalline tungsten carbide	550	15 500	0.21

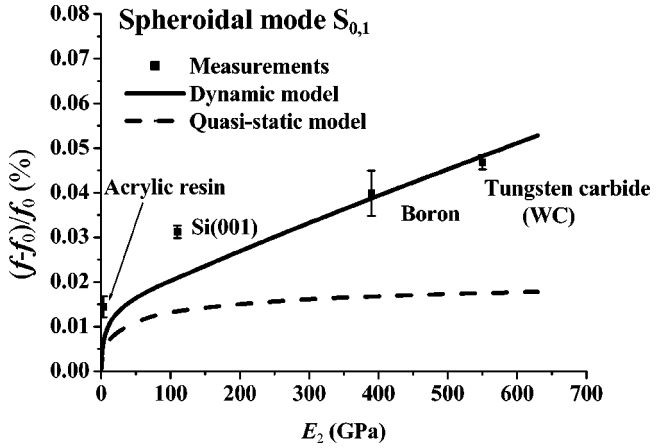

FIG. 8. Resonant-frequency shift of mode $S_{0,1}$ for the case of two-point contact.

VI. CONCLUSION

Based on the assumption of small vibrational amplitude, an approximate dynamic contact model was presented to investigate the high-frequency free vibration of a uniform elastic sphere contacting two semi-infinite viscoelastic solids. Numerical results of the dynamic model reveal that the resonant frequencies are mainly affected by Young's modulus and Poisson's ratio of contacting specimens, not by the mass density and internal friction of the contacting materials. The frequency shifts predicted by the present dynamic model agreed with those measured by electromagnetic–acoustic resonance for $S_{0,1}$ mode. However, the quasistatic model, which is conventionally used, predicted much smaller frequency shifts.

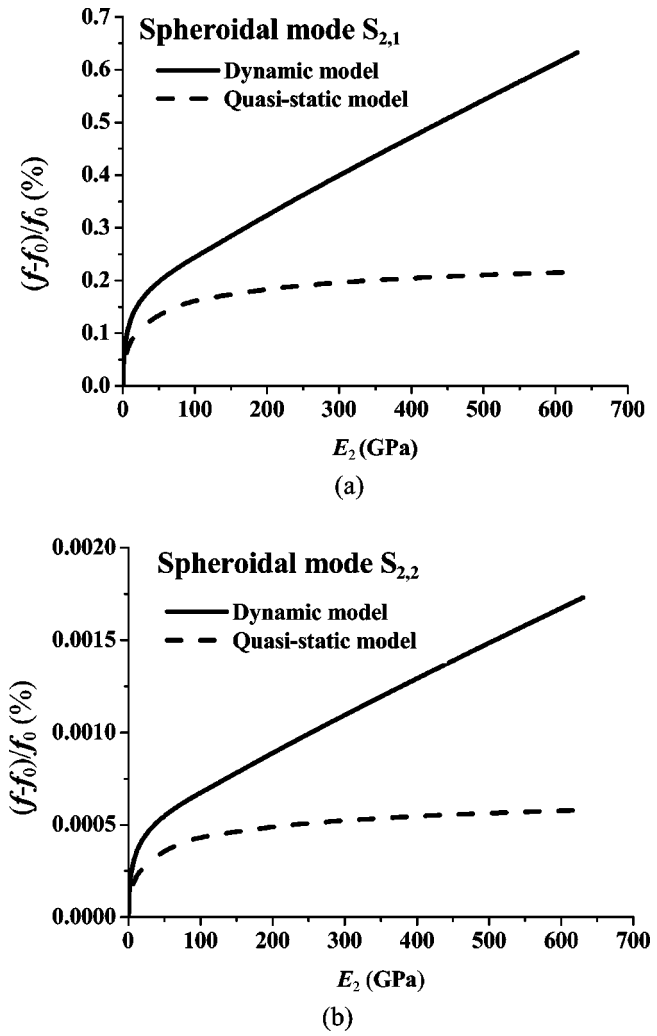

FIG. 9. Resonant-frequency shifts of modes $S_{2,1}$ and $S_{2,2}$ for the case of two-point contact.

ACKNOWLEDGMENT

The first author (J.T.) acknowledges the support provided by the Japan Society for the Promotion of Science (JSPS).

APPENDIX A: FORMULAS IN SPHERICAL COORDINATES (r,θ,ϕ) (Ref. 13)

Displacement potential relationships

$$u_r=\frac{\partial\varphi}{\partial r}+\frac{1}{k_S}\left[\frac{\partial^2(r\chi)}{\partial r^2}-r\nabla^2\chi\right],$$

$$u_\theta=\frac{1}{r}\frac{\partial\varphi}{\partial\theta}+\frac{1}{r\sin\theta}\frac{\partial^2(r\xi)}{\partial\phi}+\frac{1}{k_S r}\frac{\partial^2(r\chi)}{\partial\theta\partial r},$$

$$u_\phi=\frac{1}{r\sin\theta}\frac{\partial\varphi}{\partial\phi}-\frac{1}{r}\frac{\partial(r\xi)}{\partial\theta}+\frac{1}{k_S r\sin\theta}\frac{\partial^2(r\chi)}{\partial\phi\partial r},$$

where

$$\nabla^2=1/r^2[\partial(r^2\partial/\partial r)/\partial r]+[1/r^2\sin(\theta)]\times[\partial(\sin\theta\partial/\partial\theta)/\partial\theta]+[1/r^2\sin^2\theta]\partial^2/\partial\phi^2.$$

φ and χ are related to spheroidal vibration of elastic sphere. Torsional vibration of elastic sphere is denoted by ξ, which is not considered and set to be zero in this paper.

Stress in terms of displacement potentials

$$\sigma_{rr}=\lambda\nabla^2\varphi+2\mu\frac{\partial^2\varphi}{\partial r^2}+\frac{2\mu}{k_S}\frac{\partial}{\partial r}\left[\frac{\partial^2(r\chi)}{\partial r^2}-r\nabla^2\chi\right],$$

$$\sigma_{r\theta}=\frac{2\mu}{r}\left[\frac{\partial^2\varphi}{\partial r\partial\theta}-\frac{1}{r}\frac{\partial\varphi}{\partial\theta}\right]-\frac{\mu}{r}\left[\frac{1}{r\sin\theta}\frac{\partial(r\xi)}{\partial\phi}-r\frac{\partial}{\partial r}\left(\frac{1}{r\sin\theta}\frac{\partial(r\xi)}{\partial\phi}\right)\right]+\frac{\mu}{k_S r}\left[\frac{\partial}{\partial\theta}\left(\frac{\partial^2(r\chi)}{\partial r^2}-r\nabla^2\chi\right)-\frac{1}{r}\frac{\partial^2(r\chi)}{\partial\theta\partial r}+r\frac{\partial}{\partial r}\left(\frac{1}{r}\frac{\partial^2(r\chi)}{\partial\theta\partial r}\right)\right],$$

$$\sigma_{r\phi}=2\mu\left[\frac{1}{r\sin\theta}\frac{\partial^2\varphi}{\partial r\partial\phi}-\frac{1}{r^2\sin\theta}\frac{\partial\varphi}{\partial\phi}\right]+\mu\left[\frac{2}{r^2}\frac{\partial(r\xi)}{\partial\theta}-\left(\frac{1}{r}\frac{\partial^2(r\xi)}{\partial r\partial\theta}\right)\right]+\frac{\mu}{k_S}\left[\frac{1}{r\sin\theta}\frac{\partial}{\partial\phi}\left(\frac{2\partial^2(r\chi)}{\partial r^2}-r\nabla^2\chi\right)-\frac{1}{r^2\sin\theta}\frac{\partial^2(r\chi)}{\partial\phi\partial r}\right].$$

APPENDIX B: EXPRESSIONS FOR $C_{m1}(r)-C_{m6}(r)$ AND $D_{m1}(r)-D_{m6}(r)$

$$C_{m1}(r)=\frac{dj_m(k_Lr)}{dr},$$

$$C_{m2}(r)=\frac{j_m(k_Lr)}{r},$$

$$C_{m3}(r)=0,$$

$$C_{m4}(r)=\left((\lambda+2\mu)\frac{d^2j_m(k_Lr)}{dr^2}+\lambda\left(2\frac{dj_m(k_Lr)}{rdr}-\frac{j_m(k_Lr)(m^2+m)}{r^2}\right)\right),$$

$$C_{m5}(r)=2\mu\left(\frac{dj_m(k_Lr)}{rdr}-\frac{j_m(k_Lr)}{r^2}\right),$$

$$C_{m6}(r)=0,$$

$$D_{m1}(r)=\frac{m(m+1)}{k_Sr}j_m(k_Sr),$$

$$D_{m2}(r)=\frac{d(rj_m(k_Sr))}{k_Srdr},$$

$$D_{m3}(r)=0,$$

$$D_{m4}(r)=2\mu m(m+1)\left(\frac{2dj_m(k_Sr)}{k_Srdr}-\frac{j_m(k_Sr)}{k_Sr^2}\right),$$

$$D_{m5}(r)=\mu\left(\frac{d^2j_m(k_Sr)}{k_Sdr^2}+\frac{j_m(k_Sr)(m^2+m-2)}{k_Sr^2}\right),$$

$$D_{m6}(r)=0.$$

APPENDIX C: EXPRESSIONS FOR $S_{m1}-S_{m4}$ AND $T_{m1}-T_{m4}$

$$S_{m1}=\frac{N_{21}(a_1)D_{m1}(R)-N_{21}(0)D_{m1}(R)P_m^0(\cos(a_1/R))}{N_{11}(0)N_{21}(a_1)-N_{21}(0)N_{11}(a_1)},$$

$$S_{m2}=\frac{N_{11}(a_1)D_{m1}(R)-N_{11}(0)D_{m1}(R)P_m^0(\cos(a_1/R))}{N_{11}(0)N_{21}(a_1)-N_{21}(0)N_{11}(a_1)},$$

$$S_{m3}=\frac{N_{22}(a_2)D_{m1}(R)(-1)^m-N_{22}(0)D_{m1}(R)P_m^0(\pi-\cos(a_2/R))}{N_{12}(0)N_{22}(a_2)-N_{22}(0)N_{12}(a_2)},$$

$$S_{m4}=\frac{N_{12}(a_2)D_{m1}(R)(-1)^m-N_{12}(0)D_{m1}(R)P_m^0(\pi-\cos(a_2/R))}{N_{12}(0)N_{22}(a_2)-N_{22}(0)N_{12}(a_2)},$$

$$T_{m1}=\frac{N_{21}(a_1)C_{m1}(R)-N_{21}(0)C_{m1}(R)P_m^0(\cos(a_1/R))}{N_{11}(0)N_{21}(a_1)-N_{21}(0)N_{11}(a_1)},$$

$$T_{m2}=\frac{N_{11}(a_1)C_{m1}(R)-N_{11}(0)C_{m1}(R)P_m^0(\cos(a_1/R))}{N_{11}(0)N_{21}(a_1)-N_{21}(0)N_{11}(a_1)},$$

$$T_{m3}=\frac{N_{22}(a_2)C_{m1}(R)(-1)^m-N_{22}(0)C_{m1}(R)P_m^0(\pi-\cos(a_2/R))}{N_{12}(0)N_{22}(a_2)-N_{22}(0)N_{12}(a_2)},$$

$$T_{m4}=\frac{N_{12}(a_2)C_{m1}(R)(-1)^m-N_{12}(0)C_{m1}(R)P_m^0(\pi-\cos(a_2/R))}{N_{12}(0)N_{22}(a_2)-N_{22}(0)N_{12}(a_2)}.$$

[1] K. Yamanaka and S. Nakano, Appl. Phys. A: Mater. Sci. Process. **66**, S313 (1998).
[2] H. Ogi, J. Tian, T. Tada, and M. Hirao, Appl. Phys. Lett. **83**, 464 (2003).
[3] J. Tian, H. Ogi, T. Tada, and M. Hirao, J. Appl. Phys. **94**, 6472 (2003).
[4] J. Tian, H. Ogi, T. Tada, and M. Hirao, J. Acoust. Soc. Am. **115**, 630 (2004).
[5] G. Gladwell, J. Sound Vib. **8**, 215 (1968).
[6] P. Nayak, J. Sound Vib. **22**, 297 (1972).
[7] D. Hess and A. Soom, J. Tribol. **113**, 80 (1991).
[8] J. Sabot, P. Krempf, and C. Janolin, J. Sound Vib. **219**, 359 (1998).
[9] E. Rigaud and J. Perret-Liaudet, J. Sound Vib. **265**, 289 (2003).
[10] W. Johnson, S. Norton, F. Bendec, and R. Pless, J. Acoust. Soc. Am. **91**, 2637 (1992).
[11] C. J. Cornejo C'ordova, *Elastodynamics with Hysteretic Damping* (Proefschrift, Technische Universiteit Delft, Holland, 2002).
[12] K. L. Johnson, *Contact Mechanics* (Cambridge University Press, Cambridge, 1985).
[13] Y. H. Pao and C. C. Mow, *Diffraction of Elastic Wave and Dynamic Stress Concentrations* (Crane, Russak, New York, 1973).
[14] B. M. Ari and J. S. Sarva, *Seismic Waves and Sources* (Springer, New York, 1981).
[15] J. D. Achenbach, *Wave Propagation in Elastic Solids* (North-Holland, Amsterdam, 1973).
[16] K. Graff, *Wave Motion in Elastic Solids* (Clarendon, Oxford, 1975).
[17] J. Miklowitz, *The Theory of Elastic Waves and Wave Guides* (North-Holland, Amsterdam, 1973).
[18] E. M. Ewing, W. S. Jardetzky, and F. Press, *Elastic Waves in Layered Media* (McGraw-Hill, New York, 1957).
[19] Y. Lou and T. Su, J. Acoust. Soc. Am. **63**, 1402 (1978).
[20] W. Jonson, J. Appl. Phys. **83**, 2462 (1998).
[21] M. Hirao, H. Ogi, and H. Fukuoka, Rev. Sci. Instrum. **64**, 3198 (1993).
[22] H. Ogi, H. Ledbetter, S. Kim, and M. Hirao, J. Acoust. Soc. Am. **106**, 660 (1999).
[23] M. Hirao and H. Ogi, *EMATs for Science and Industry: Noncontacting Ultrasonic Measurements* (Kluwer Academic, Boston, 2003).